

Complexity Project: The Oslo Model

CID: 01865474

20th February 2023

Abstract

A simulation of the Oslo Model was constructed to investigate the avalanche-size probability for a range of system sizes. It has been shown that the model is consistent with the finite-size scaling ansatz and shows self-organised criticality. Values of $D = 2.09 \pm 0.10$ and $\tau_s = 1.52 \pm 0.01$ were estimated via a data collapse of the avalanche-size distribution and were validated using a moment analysis, yielding $D = 2.13 \pm 0.01$ and $\tau_s = 1.54 \pm 0.04$.

Word Count

Approximately 2,500 excluding references, abstract and captions

Introduction

A complex system is one containing many elements interacting with each other, resulting in global dynamics different to that of any one part. Such systems are studied in several, vastly different, fields such as biology and ecology, where a flock of starlings and heart muscles can be considered complex systems, as well as electrical power networks and earthquake behaviours [1]. In this study we investigate the properties of avalanches through the two-dimensional Oslo rice pile model.

Criticality is a property of a complex system within which the components display ‘scale-invariant fluctuations’. Normally, this criticality is achieved by fine-tuning a control parameter to the point at which it is known to occur. In nature, however, complex systems can achieve criticality without the tuning of parameters. This is known as self-organised criticality (SOC) [2]. The aim of studying complex systems is to understand the mechanisms causing this scale-free behaviour in Nature [3].

1. Implementation of the Oslo Model

The Oslo Model is a two-dimensional avalanche simulation algorithm, where, starting from the ‘empty state’, the system, of size L , is driven by adding one grain at a time to site $i = 1$. For each site, $i \in \{1, 2, \dots, L\}$, there is a gradient given by $z_i = n_i - n_{i+1}$, where n_i is the number of grains at that site, and randomly chosen threshold gradient $z_i^{thresh} \in \{1, 2\}$. n_{L+1} is held at 0 and in the Oslo Model the probability of picking $z_i^{thresh} = 1$ or 2 is $\frac{1}{2}$. After each grain addition, if $z_i > z_i^{thresh}$ that site is relaxed according to the following transformations.

For $i = 1$:

$$z_1 \rightarrow z_1 - 2 \quad (1.1)$$

$$z_2 \rightarrow z_2 + 1 \quad (1.2)$$

For $i = 2, \dots, L - 1$:

$$z_i \rightarrow z_i - 2 \quad (1.3)$$

$$z_{i \pm 1} \rightarrow z_{i \pm 1} + 1 \quad (1.4)$$

For $i = L$:

$$z_L \rightarrow z_L - 1 \quad (1.5)$$

$$z_{L-1} \rightarrow z_{L-1} + 1 \quad (1.6)$$

After site i is relaxed, z_i^{thresh} is randomised again. After all sites are relaxed, the system is driven once more, and the process is iterated. The avalanche size, s , is the number of relaxations that occur per grain added to the system [3].

To check the algorithm was working as intended, the steady state height at site $i = 1$ averaged over time was measured for $L = 16$ and $L = 32$ systems and compared to expected values, shown in table 1. The average was taken over 700 iterations for $L = 16$, and 1000 iterations for $L = 32$.

Table 1 - Initial validation of the Oslo Model implementation, comparing the measured average height in the steady state for systems of size 16 and 32 to expected values.

L	Expected average height [3]	Measured average height
16	26.5	26.75
32	53.9	53.92

The Oslo Model is a specific case of the Bak-Tang-Wiesenfeld Model (BTW), where the probability of z_i^{thresh} being a 1 or a 2 is equal. In the BTW, one can choose the probability of z_i^{thresh} being a 1 or a 2.

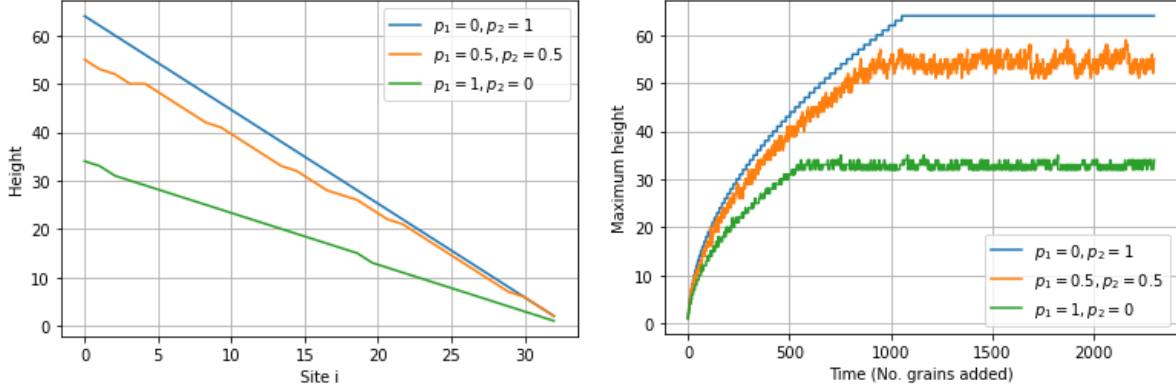


Figure 1 - Three cases of the BTW Model are considered for a system of $L=32$. Case 1: The probability of the threshold slope being a 1 is 0. Case 2: The probability of the threshold slope being a 1 is 0.5. Case 3: The probability of the threshold slope being a 1 is 1. Left: The height distribution of the piles in the steady state. Right: The height of the pile at $i=1$ as a function of the number of grains added.

The left plot shows how the height distribution of the Oslo model lies between the BTW Case 1 and Case 2, as expected. It lies closer to Case 1 because in the Oslo Model, whilst the probability of a newly generated z_i^{thresh} being a 1 or a 2 is equal, a $z_i^{thresh} = 2$ has a longer lifetime than a $z_i^{thresh} = 1$ as a site is less likely to have a larger gradient. From the right plot, one can see that Case 1 takes the longest time to reach the steady state, followed by Case 2 and then Case 3. This is as expected because with a larger threshold gradient, more grains can fit into the system before they start leaving the system at site $i = L = 32$. Furthermore, the maximum height of the pile at the steady state should be around 64 for Case 1 and 32 for Case 2, which is observed in both plots. This was consistent for $L = \{4,8,16,32,64,128,256\}$.

2. The Height of the Pile $h(t;L)$

2.1 Transient and Recurrent Configurations

After a grain is added to the pile, the system relaxes fully to a stable configuration. There are two types of stable configurations: transient and recurrent. Transient configurations occur just once and only before stable configurations are reached. Recurrent configurations occur when the system is ‘filled’ and reaches its maximum height, which is limited by L . At this point the average number of grains added to the system is equal to the average number of grains leaving the system – a result of most z_i being equal to the average z_i^{thresh} leading to avalanches effectively forcing new grains down the ‘staircase’ and out the other side. This is described by equation (2).

$$\underbrace{\mathcal{T}_0 \mapsto \mathcal{T}_1 \mapsto \cdots \mapsto \mathcal{T}_{n-1}}_{\text{transient configurations}} \mapsto \underbrace{\mathcal{R}_n \mapsto \mathcal{R}_{n+1} \mapsto \cdots}_{\text{recurrent configurations}}. \quad (2)$$

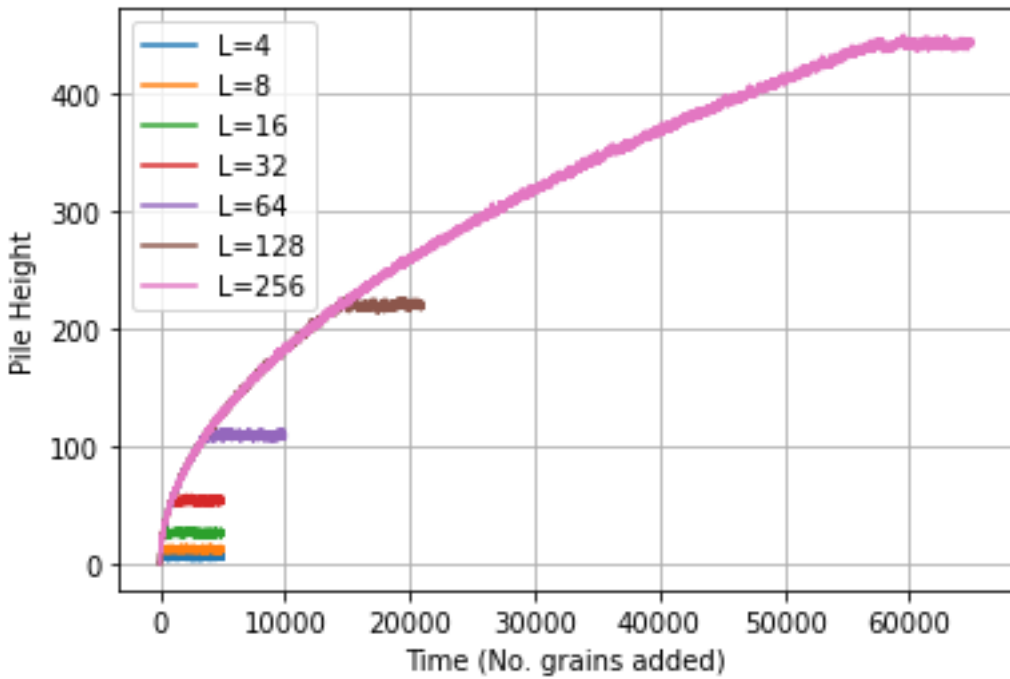


Figure 2 - Pile height as a function of the number of grains added for a range of system sizes.

Figure 2 shows the time at which transient configurations (positive gradient) and recurrent configurations occur for a range of system sizes. As expected, the larger the system the longer it takes to achieve the steady state.

2.2 Average Cross-over Time

The cross-over time, $t_c(L)$, is the number of grains added to the system before a grain added induces a grain to leave the system. $t_c(L)$ was measured 10 times for each system size and was then averaged to give $\langle t_c(L) \rangle$, plotted on the left in figure 3 as a function of system size. A quadratic curve was fitted to the data points, implying $\langle t_c(L) \rangle \propto L^2$.

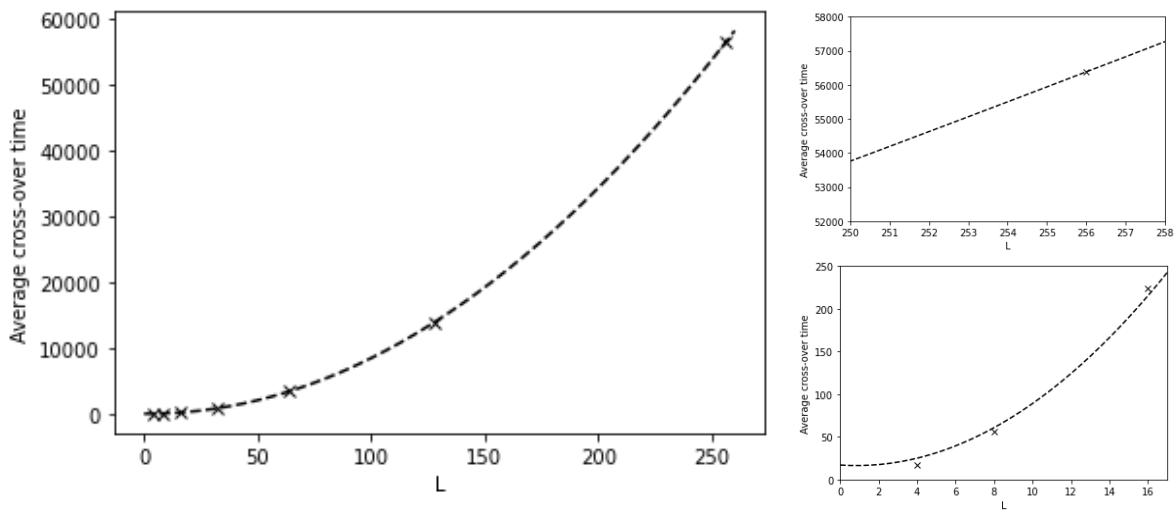


Figure 3 - Left: The average cross-over time as a function of system size. Right: Subplots of the left, showing the three smallest system sizes (top) and the largest system size (bottom).

The plots on the right in figure 3 show how the cross-over time for smaller systems deviate further from the quadratic fit than that of the largest system. This suggest that the scaling relationship only holds for $L \gg 1$.

2.3 Height and Average Cross-over Time Scaling with System Size

2.3.1 Height Scaling with System Size

The height of the pile at a time t is given by equation (3.1) and, for $L \gg 1$, the average height can be shown to be proportional to L as follows.

$$h(t; L) = \sum_{i=1}^L z_i(t) \quad (3.1)$$

$$\langle h(t; L) \rangle = \sum_{i=1}^L \langle z_i(t) \rangle \quad (3.2)$$

$$\langle h(t; L) \rangle = L \langle z_i(t) \rangle \quad \text{for } L \gg 1 \quad (3.3)$$

2.3.2 Cross-over Time Scaling with System Size

The cross-over time is shown in equation (4.1) and is used to derive a scaling relationship between the average cross-over time and system size.

$$t_c(L) = \sum_{i=1}^L z_i \cdot i \quad (4.1)$$

$$\langle t_c(L) \rangle = \sum_{i=1}^L \langle z_i \cdot i \rangle \quad (4.2)$$

$$\langle t_c(L) \rangle = L \langle z_i \rangle \langle i \rangle \quad (4.3)$$

$$\langle t_c(L) \rangle = \langle z_i \rangle \frac{L^2}{2} \quad (4.4)$$

as $\langle i \rangle \approx \frac{L}{2}$ for $L \gg 1$. It has been shown that $\langle t_c(L) \rangle \propto L^2$, which is consistent with the measured values in figure 3.

2.4 Data Collapse for the Processed Height

To produce a data collapse for the height of the piles as a function of time, first the processed height, $\tilde{h}(t; L)$, was calculated for each system size to smooth out the data.

Effectively this is an average of $h(t; L)$ taken over 5 realisations for each L . As $\tilde{h}(t; L) \propto L$ and $t_c \propto L^2$ these values were divided by L and L^2 respectively to make both axis invariant in L . The data collapse is shown in figure 4 and is described by the scaling function in equation (5).

$$\tilde{h}(t; L) = L F\left(\frac{t}{L^2}\right) \quad (5)$$

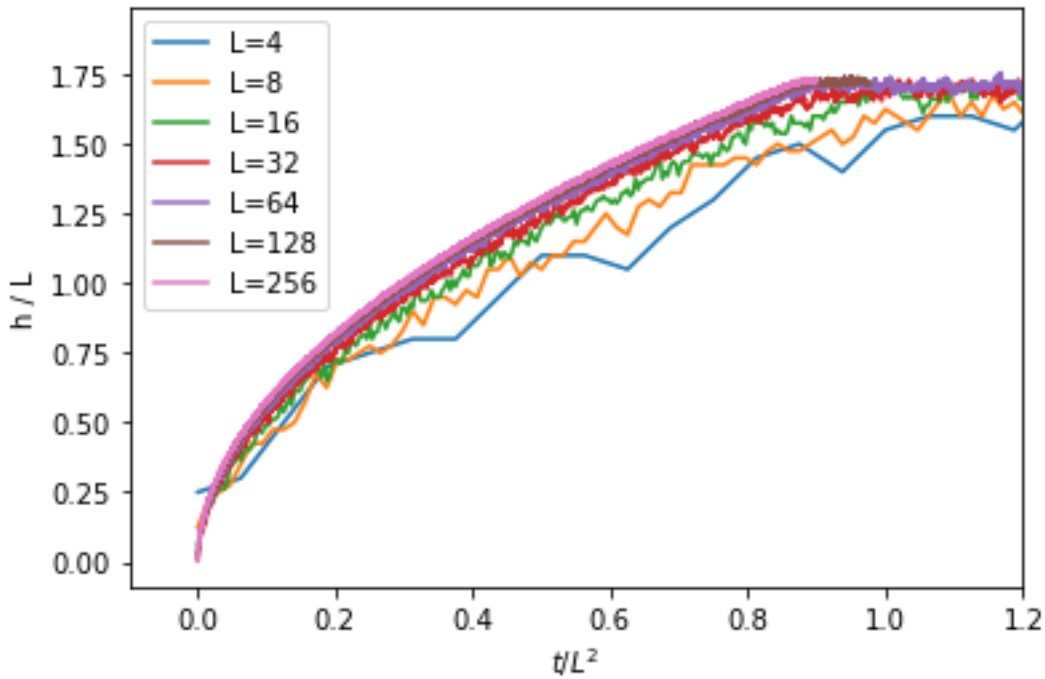


Figure 4 - A data collapse for the processed height as a function of time for a range of system sizes.

As seen in figure 4, the scaling function behaves like equation (6). The smaller systems deviate from this scaling function as the proportionality arguments only hold for $L \gg 1$.

$$F(x) = \begin{cases} \sqrt{x} & x \ll 1 \\ \langle z_i \rangle & x \gg 1 \end{cases} \quad (6)$$

This is because, during the transient, the height must increase at a decreasing rate, due to the increasing probability of larger avalanches as the number of grains in the system increases. For $x \gg 1$, $t > t_c$ hence the steady state has been reached. The recurrent solution can be found by comparing figure 4 to equation (3.3).

From the scaling function, it can be deduced that in the transient $\tilde{h}(t; L) \propto \sqrt{t}$, as follows.

$$\frac{\tilde{h}(t; L)}{L} \propto \sqrt{\frac{t}{L^2}} \quad (7.1)$$

$$\tilde{h}(t; L) \propto \sqrt{t} \quad (7.2)$$

2.5 Corrections to Scaling

The scaling function, equation 5, can only be applied to systems with $L \gg 1$. Furthermore, it would only perfectly describe a system in the thermodynamic limit, $L \rightarrow \infty$. This is the root of the corrections to scaling and is illustrated in figure 4, where the smallest systems lie furthest below the scaling function.

To investigate the corrections to scaling of the average height of a system, only $h(t; L)$ for $t > t_c(L)$ was considered. 10,000 grains were added into each system after the

steady state was achieved, and this is the time that the height was averaged over. The form of the corrections to scaling was assumed to be given by equation (8)

$$\langle h(t; L) \rangle = a_0 L (1 - a_1 L^{-\omega_1}) \quad (8)$$

where $\omega_1 > 0$ and a_i are constants, and $\langle h(t; L) \rangle$ is the mean recurring configuration height. When $L \gg 1$, equation (8) can be approximated as equation (9), which, using equation (3.3) implies $a_0 = \langle z_i \rangle$. This equation was fitted to figure 5 (left) to deduce a value for $a_0 = 1.727 \pm 0.004$. Only $L = \{64, 128, 256\}$ were considered when fitting.

$$\langle h(t; L) \rangle = a_0 L \quad (9)$$

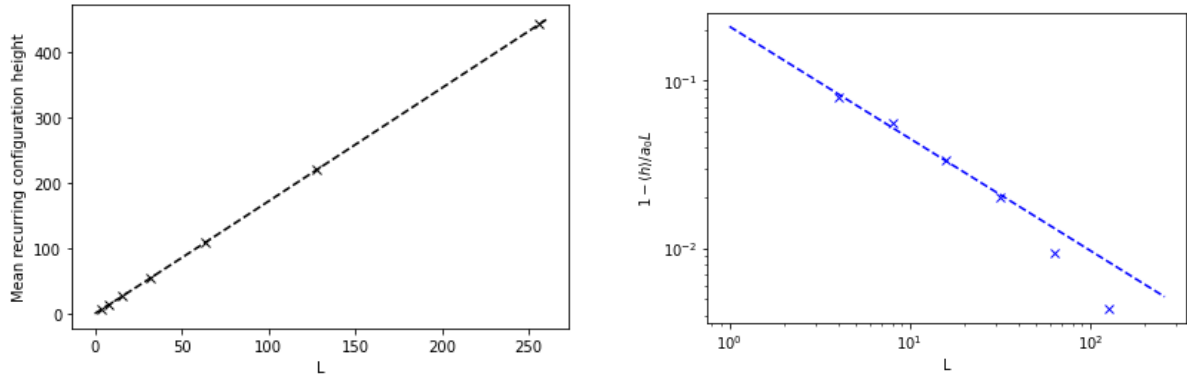


Figure 5 – Left: Mean recurring configuration height as a function of system size, with a fit of equation (9) to find a_0 . Right: A log-log plot of the transformed height with a fit of equation (10) to find ω_1 .

To extract a value for ω_1 , equation (8) is rearranged to equation (10). Then, plotting $1 - \frac{\langle h(t; L) \rangle}{a_0 L}$ against L on a logarithmic graph, shown in figure 5 (right), and fitting equation (10) to the data points gives a negative gradient and $\omega_1 = 0.667 \pm 0.042$. Only $L = \{4, 8, 16, 32\}$ were considered for this fit, as these are the systems more affected by corrections to scaling, and the previously extracted value of a_0 was used.

$$\log \left(1 - \frac{\langle h(t; L) \rangle}{a_0 L} \right) = \log(a_1) - \omega_1 \log(L) \quad (10)$$

2.6 σ_h , $\sigma_{\langle z \rangle}$ and $\langle z_i \rangle$

The standard deviation of the height was measured for each system, shown in figure 6 (left) where it is initially fitted using equation (11)

$$\sigma_h = b\sqrt{L} + c \quad (11)$$

where b and c are constants.

Further analysis was done to calculate the scaling relationship between σ_h and L . By fitting a power law relationship through a logarithmic plot of the data points, shown in figure 6 (right), it was deduced that $\sigma_h \propto L^{0.18}$ with negligible uncertainty.

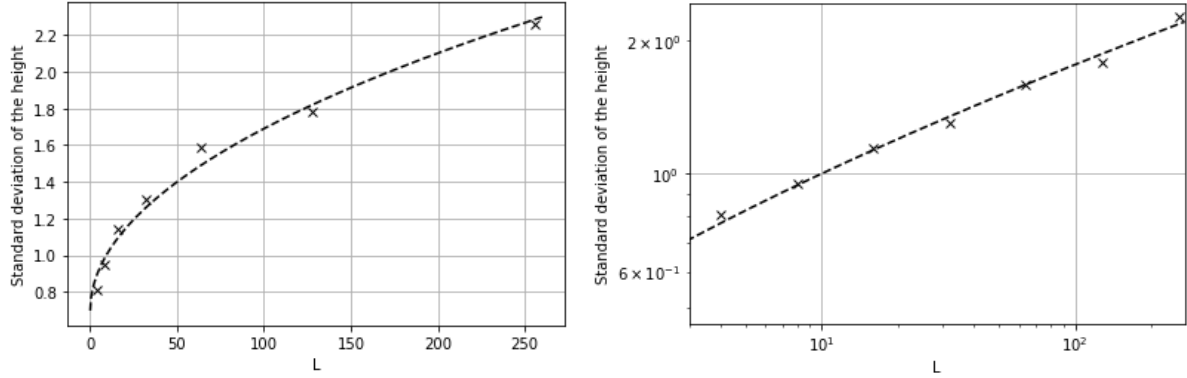


Figure 6 - Left: The standard deviation of the height against L , fitted with a square root. Right: The standard deviation of the height against L on a logarithmic plot used to deduce the proper scaling relationship.

Using equation (3.3), the corresponding propagation of errors is shown in equation (12.1),

$$\frac{\sigma_{\langle z \rangle}}{\langle z \rangle} = \sqrt{\left(\frac{\sigma_h}{h}\right)^2 + \left(\frac{\sigma_L}{L}\right)^2} \quad (12.1)$$

and, since $\sigma_L = 0$, one can show that

$$\sigma_{\langle z \rangle} = \frac{\langle z \rangle \sigma_h}{h} = \frac{\sigma_h}{L}, \quad (12.2)$$

Hence $\sigma_{\langle z \rangle} \propto L^{-0.82}$. As $L \rightarrow \infty$, $\sigma_{\langle z \rangle} \rightarrow 0$.

Using equation (8) in the limit $L \rightarrow \infty$, given by equation (9), $\langle z \rangle \rightarrow a_0$.

2.7 Height Probability

Assuming z_i are independent, identically distributed random variables with finite variance, and $h = \sum_{i=1}^L z_i$, according to the central limit theorem, one would expect the height probability, $P(h; L)$, to have a gaussian distribution for $L \gg 1$ of the form shown in equation (13).

$$P(h; L) = \frac{1}{\sigma_h \sqrt{2\pi}} e^{-\frac{(h-\langle h \rangle)^2}{2\sigma_h^2}} \quad (13)$$

Since z_i are independent, identically distributed random variables with a finite variance, it can be assumed that $\sigma_h^2 = \sum_{i=1}^L \sigma_z^2 = L\sigma_z^2$. Hence, $\sigma_h \propto \sqrt{L}$.

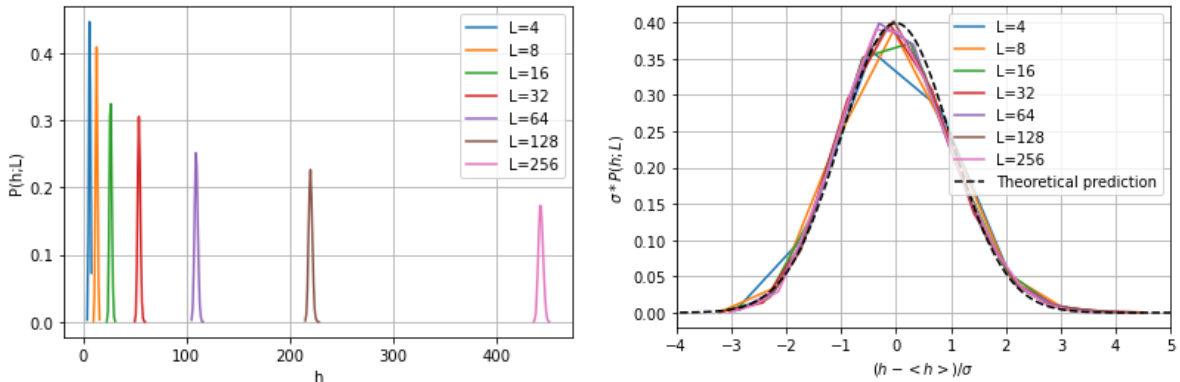


Figure 7 – Left: A plot of the height probability distribution, calculated over 10,000 recurrent configurations for each system size. Right: A data collapse for the height probability distribution with the theoretically predicted equation (14) in black.

In figure 7, equation (13) has been used to produce a data collapse for the height probability distribution. Under the transformations $P(h; L) \rightarrow \sigma_h P(h; L)$ and $h \rightarrow \frac{(h-\langle h \rangle)}{\sigma_h}$, the distribution is expected to have the form

$$y = \frac{1}{\sqrt{2\pi}} e^{-\frac{1}{2}x^2}, \quad (14)$$

with a mean, $\mu = 0$, and a standard deviation, $\sigma = 1$.

Initially, by fitting a gaussian of the form of equation (13) onto the data collapse, it is found that $\mu = -0.05 \pm 0.01$ and $\sigma = 1.00 \pm 0.01$. Whilst the standard deviation lies within the expected value, the mean demonstrates deviation from the theoretical prediction. Furthermore, figure 7 (right) shows the positive skew of the data collapse in comparison to the theoretically predicted gaussian curve. This implies that z_i are not independent, identically distributed random variables with a finite variance. They are dependent on each other because an avalanche at one site can lead to a change of slope at another site.

Should all z_i be regenerated randomly, with a reasonable variance, after each grain addition, one would expect the data collapse to better fit the theoretical prediction.

3. The Avalanche-Size Probability $P(s; L)$

3.1 Data Collapse for Avalanche-Size Probability

To perform a data collapse of the avalanche-size probability distribution, shown in figure 8 (left), the avalanche sizes over 10^6 grains added to the steady state were measured for each system size. The avalanche sizes were then converted to the probability distribution via a log-binning method, binning the data in logarithmically growing bin sizes, to reduce the noise of the data and enhance the physical features of the distribution. This method was controlled by a scale parameter of 1.5. Avalanches of $s = 0$ were not included in this method due to their incompatibility with the logarithmic plot.

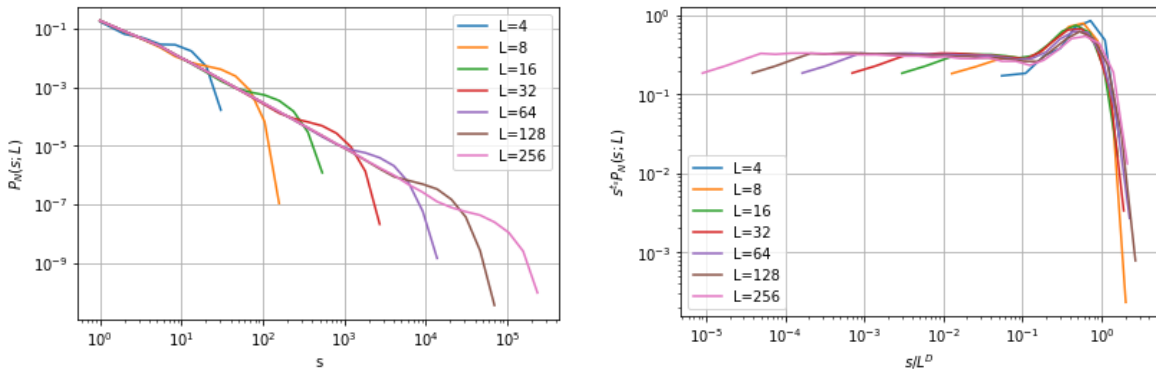


Figure 8 - Left: Avalanche-size probability distribution as a function of avalanche size for all system sizes. Right: The data collapse for the avalanche-size probability distribution, $D=2.09$, $\tau_s=1.52$.

The SOC property of the Oslo Model is clearly visible in figure 8 (left) as the distributions lie on top of each other, demonstrating the scale-invariance of the system. The ‘bump’ in the distributions is thought to be due to ‘system spanning avalanches where grains are dropping out at the right boundary’ [3]. For each system size, the avalanche-size

probability decreases with avalanche size until a cut-off avalanche size is reached, at which point there is a rapid decay in the probability. The larger the system, the larger the cut-off avalanche size. A finite-size scaling ansatz, shown in equation (15), can be used to describe the distributions.

$$P_N(s; L) \propto s^{-\tau_s} G\left(\frac{s}{L^D}\right) \quad (15)$$

where D is the avalanche dimension and τ_s is the avalanche-size exponent.

The data collapse, shown in figure 8 (right), was achieved using a two-step process. First, the data was collapsed in the y-axis via the transformation $P_N(s; L) \rightarrow s^{\tau_s} P_N(s; L)$. Given $-\tau_s$ is the gradient of the un-collapsed distribution, and the ansatz holds for $L \gg 1$, τ_s was found by fitting a straight line to the linear part of the $L = 256$ distribution. It was found that $\tau_s = 1.52 \pm 0.01$. Second, the data was collapsed in the x-axis via the transformation $s \rightarrow \frac{s}{L^D}$. This was done by eye, iterating through a range of possible D values until the distributions aligned. It was found that $D = 2.09 \pm 0.10$. The relatively large uncertainty here is to account for human error.

3.2 Moment Analysis

The k 'th moment, $\langle s^k \rangle$, is defined as

$$\langle s^k \rangle = \lim_{T \rightarrow \infty} \frac{1}{T} \sum_{t=t_0+1}^{t_0+T} s_t^k, \quad (16)$$

where s_t is the measured avalanche size at time t and $t_0 > t_c(L)$. This was measured directly for $k = \{1, 2, 3, 4\}$, with $T = 10^6$.

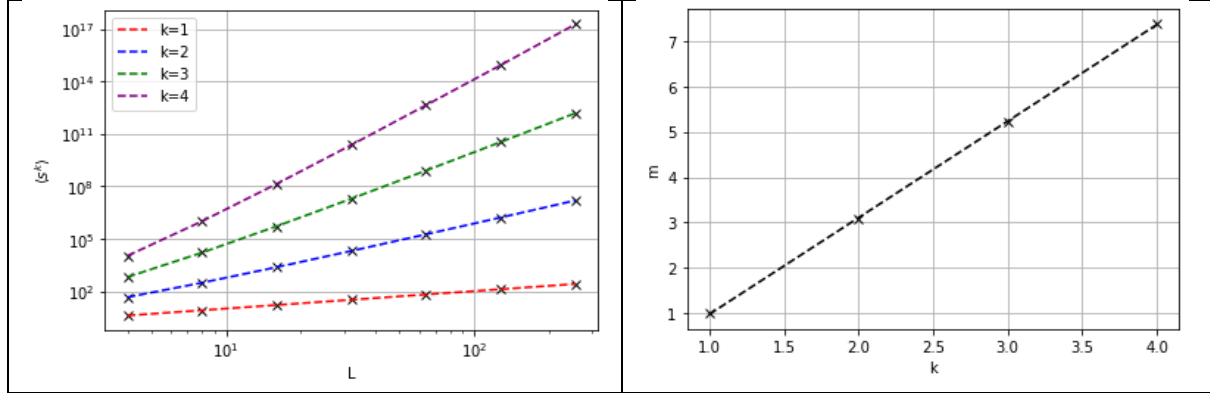


Figure 9 – Left: The k 'th moment plotted against L for $k=\{1,2,3,4\}$. Right: $m=D(1+k-\tau_s)$ plotted against k , fitted with a straight line.

Using equation (17.1) with the ansatz in equation (15) and the substitution $u = \frac{s}{L^D}$, one can show that $\langle s^k \rangle \propto L^{D(1+k-\tau_s)}$.

$$\langle s^k \rangle = \sum_{s=1}^{\infty} s^k P_N(s; L) \quad (17.1)$$

$$\langle s^k \rangle = \sum_{s=1}^{\infty} s^{k-\tau_s} G\left(\frac{s}{L^D}\right) \quad (17.2)$$

$$\langle s^k \rangle \approx \int_1^{\infty} s^{k-\tau_s} G\left(\frac{s}{L^D}\right) ds \quad (17.3)$$

$$\langle s^k \rangle \approx L^{D(1+k-\tau_s)} \int_{1/L^D}^{\infty} u^{k-\tau_s} G(u) du \quad (17.4)$$

In the limit $L \rightarrow \infty$, the integral will tend towards a constant, giving the aforementioned relationship. Taking the logarithm of equation (17.4), equation (18) is fitted in figure 9 (left), with a strong correlation to the data points.

$$\log\langle s_k \rangle = D(1 + k - \tau_s) \log(L) + \log(\text{const.}) \quad (18)$$

From this fit, the gradients $m(k) = D(1 + k - \tau_s)$ for each moment can be found to a high accuracy.

Using a plot of $m(k)$ against k , shown in figure 9 (right), the gradient, D , is found to be $D = 2.13 \pm 0.01$. The x-intercept $= \tau_s - 1$, giving a value of $\tau_s = 1.54 \pm 0.04$. The error on τ_s was calculated using the standard propagation of errors considering the fitting errors on the gradient and the y-intercept. These results are consistent with the estimates found in section 3.1. This suggests the estimation methods used were effective.

Conclusion

In conclusion, the scale-invariant property of the SOC Oslo Model was proven via data collapses of the height and the avalanche-size probability distributions. For small system sizes, corrections to scaling skewed the distributions. It was shown that z_i are not independent, identically distributed random variables with finite variance. The avalanche dimension and avalanche-size exponent were estimated and then validated using moment analysis.

References

- [1] M. Garrido (1993) *Complexity in Physics and Technology*. World Scientific
- [2] H. Hoffmann, D. Payton (2018) *Optimisation by Self-Organised Criticality*. Scientific Reports
- [3] K. Christensen (2023) *Complexity and Networks course 2022-2023: Complexity Project Notes*. Imperial College